2011 50th IEEE Conference on Decision and Control and
European Control Conference (CDC-ECC)
Orlando, FL, USA, December 12-15, 2011

Stable Manifolds of Saddle Equilibria for Pendulum Dynamics on S^2 and $\mathsf{SO}(3)$

Taeyoung Lee*, Melvin Leok†, and N. Harris McClamroch

***Abstract*— Attitude control systems naturally evolve on nonlinear configurations, such as S^2 and $\mathsf{SO}(3)$. The nontrivial topological properties of these configurations result in interesting and complicated nonlinear dynamics when studying the corresponding closed loop attitude control systems. In this paper, we review some global analysis and simulation techniques that allow us to describe the global nonlinear stable manifolds of the hyperbolic equilibria of these closed loop systems. A deeper understanding of these invariant manifold structures are critical to understanding the global stabilization properties of closed loop attitude control systems, and these global analysis techniques are applicable to a broad range of problems on nonlinear configuration manifolds.**

I. Introduction

Global nonlinear dynamics of various classes of closed loop attitude control systems have been studied in recent years [1]. Closely related results on attitude control of a spherical pendulum (with attitude an element of the two-sphere S^2) and of a 3D pendulum (with attitude an element of the special orthogonal group $\mathsf{SO}(3)$) are given in [2], [3]. These publications address the global closed dynamics of smooth vector fields on nonlinear manifolds.

Assuming that the controlled system has an asymptotically stable equilibrium, as desired in attitude stabilization problems, additional hyperbolic equilibria necessarily appear [4]. As a result, the desired equilibrium is not globally asymptotically stable, since the domain of attraction of the desired asymptotically stable equilibrium excludes the union of the stable manifolds of the hyperbolic equilibria. It is referred to as *almost* globally asymptotically stable, as the stable manifolds of the hyperbolic equilibria have lower dimension than the attitude configuration manifold. However, the characteristics of the stable manifolds to the hyperbolic equilibria and the corresponding effects on the solutions have not been directly studied in the prior literatures.

These geometric factors motivate the current paper, in which new computational results to visualize the stable manifolds of the hyperbolic equilibria are developed. To make the development concrete, the presentation is built around two specific closed loop vector fields: one for the attitude dynamics of a spherical pendulum and one for the attitude dynamics of a 3D pendulum. While the observations in this paper are based on two particular examples, the computational results suggest that the existence of the hyperbolic equilibria may have nontrivial influences on the solutions of any attitude control system, even though their stable manifolds have zero measure. Further studies are required to understand the effects of the hyperbolic equilibria completely. Another contribution of this paper is that the presented computational tools are also broadly applicable to studying the geometry of more general control systems on nonlinear manifolds.

Taeyoung Lee, Mechanical and Aerospace Engineering, George Washington University, Washington DC 20052 tlee@gwu.edu

Melvin Leok, Mathematics, University of California at San Diego, La Jolla, CA 92093 mleok@math.ucsd.edu

N. Harris McClamroch, Aerospace Engineering, University of Michigan, Ann Arbor, MI 48109 nhm@umich.edu

*This research has been supported in part by NSF under grants CMMI-1029551.

†This research has been supported in part by NSF under grants DMS-0726263, DMS-1001521, DMS-1010687, and CMMI-1029445.

II. Spherical Pendulum

A spherical pendulum is composed of a mass m connected to a frictionless pivot by a massless link of length l. It is acts under uniform gravity, and it is subject to a control moment u. The configuration of a spherical pendulum is described by a unit-vector $q \in \mathbb{R}^3$, representing the direction of the link with respect to a reference frame.

Therefore, the configuration space is the two-sphere $\mathsf{S}^2 = \{q \in \mathbb{R}^3 \,|\, q \cdot q = 1\}$. The tangent space of the two-sphere at q, namely $\mathsf{T}_q\mathsf{S}^2$, is the two-dimensional plane tangent to the unit sphere at q, and it is identified with $\mathsf{T}_q\mathsf{S}^2 \simeq \{\omega \in \mathbb{R}^3 \,|\, q \cdot \omega = 0\}$, using the following kinematics equation:

$$\dot{q} = \omega \times q,$$

where the vector $\omega \in \mathbb{R}^3$ represents the angular velocity of the link. The equation of motion is given by

$$\dot{\omega} = \frac{g}{l} q \times e_3 + \frac{1}{ml^2} u,$$

where the constant g is the gravitational acceleration, and the vector $e_3 = [0, 0, 1] \in \mathbb{R}^3$ denotes the unit vector along the direction of gravity. The control moment at the pivot is denoted by $u \in \mathbb{R}^3$.

A. Control System

Several proportional-derivative (PD) type control systems have been developed on S^2 in a coordinate-free fashion [5], [6]. Here, we summarize a control system that stabilizes a spherical pendulum to a fixed desired direction $q_d \in \mathsf{S}^2$.

Consider an error function on S^2, representing the distance from the direction q to the desired direction q_d, given by

$$\Psi(q, q_d) = 1 - q \cdot q_d.$$

A control input is composed of a proportional term along the gradient of Ψ, and a derivative term and a cancelation term. For positive constants k_q, k_ω, it is given by

$$u = ml^2(-k_q q_d \times q - k_\omega \omega - \frac{g}{l} q \times e_3).$$

The corresponding closed loop dynamics are written as

$$\dot{\omega} = -k_\omega \omega - k_q q_d \times q, \tag{1}$$

$$\dot{q} = \omega \times q. \tag{2}$$

This yields two equilibrium solutions: (i) the desired equilibrium $(q, \omega) = (q_d, 0)$; (ii) additionally, there exists another equilibrium $(-q_d, 0)$ at the antipodal point.

In this paper, we analyze the local stability of each equilibrium by linearizing the closed loop dynamics to study the equilibrium structures.

B. Linearization

Here, we develop a coordinate-free form of the linearized dynamics of (1), (2). A variation of a curve $q(t)$ on S^2 is a family of curves $q^\epsilon(t)$ parameterized by $\epsilon \in \mathbb{R}$, satisfying several properties [6]. It cannot be simply written as $q^\epsilon(t) = q(t) + \epsilon \delta q(t)$ for $\delta q(t)$ in $\mathbb{R}^3$, since in general, this does not guarantee that $q^\epsilon(t)$ lies in S^2. In [7], an expression for a variation on S^2 is given in terms of the exponential map as follows:

$$q^\epsilon(t) = \exp(\epsilon \hat{\xi}(t)) q(t), \tag{3}$$

for a curve $\xi(t)$ in $\mathbb{R}^3$ satisfying $\xi(t) \cdot q(t) = 0$ for all t. The *hat map* $\hat{\cdot} : \mathbb{R}^3 \to \mathfrak{so}(3)$ is defined by the condition that $\hat{x} y = x \times y$ for any $x, y \in \mathbb{R}^3$. The resulting infinitesimal variation is given by

$$\delta q(t) = \left. \frac{d}{d\epsilon} \right|_{\epsilon=0} q^\epsilon(t) = \xi(t) \times q(t). \tag{4}$$

The variation of the angular velocity can be written as

$$\omega^\epsilon(t) = \omega(t) + \epsilon \delta\omega(t), \tag{5}$$

for a curve $\delta w(t)$ in $\mathbb{R}^3$ satisfying $q(t) \cdot w(t) = 0$ for all t. Hereafter, we do not write the dependency on time t explicitly.

Next, we substitute (4), (5) into (1), (2), and we ignore higher-order perturbation terms. Using the fact that $\xi \cdot q = \omega \cdot q = 0$, and vector identities, a coordinate-free form of the linearized equations can be written as follows:

$$\dot{x} = \begin{bmatrix} \dot{\xi} \\ \delta\dot{\omega} \end{bmatrix} = \begin{bmatrix} qq^T\hat{\omega} & I - qq^T \\ k_q \hat{q}_d \hat{q} & -k_w I \end{bmatrix} \begin{bmatrix} \xi \\ \delta\omega \end{bmatrix} = Ax, \tag{6}$$

where the state vector of the linearized controlled system is $x = [\xi; \delta\omega] \in \mathbb{R}^6$ (see [8] for detailed derivation). A spherical pendulum has two degrees of freedom, but this linearized equation of motion evolves in $\mathbb{R}^6$ instead of $\mathbb{R}^4$. Since $q \cdot \omega = 0$ and $q \cdot \xi = 0$, we have the following two additional constraints on $\xi, \delta\omega$:

$$Cx = \begin{bmatrix} q^T & 0 \\ -\omega^T \hat{q} & q^T \end{bmatrix} \begin{bmatrix} \xi \\ \delta\omega \end{bmatrix} = \begin{bmatrix} 0 \\ 0 \end{bmatrix}. \tag{7}$$

Therefore, the state vector x should lie in the null space of the matrix $C \in \mathbb{R}^{2\times 4}$. However, this is not an extra constraint that should be imposed when solving (6). As long as the initial condition $x(0)$ satisfies (7), the structure of (1), (2), and (6), guarantees that $x(t)$ satisfies (7) for all t, i.e. $\frac{d}{dt} C(t)x(t) = 0$ for all $t \geq 0$ when $C(0)x(0) = 0$.

C. Equilibrium Solutions

We choose the desired direction as $q_d = e_3$. The equilibrium solution $(q_d, 0) = (e_3, 0)$ is referred to as the hanging equilibrium, and the additional equilibrium solution $(-q_d, 0) = (-e_3, 0)$ is referred to as the inverted equilibrium. We study the eigen-structure of each equilibrium using the linearized equation (6). To illustrate the ideas, the controller gains are selected as $k_q = k_\omega = 1$.

1) Hanging Equilibrium: The eigenvalues λ_i, and the eigenvectors v_i of the matrix A at the hanging equilibrium $(e_3, 0)$ are given by

$$\lambda_{1,2} = (-1 \pm \sqrt{3}i)/2,\ \lambda_{3,4} = \lambda_{1,2},\ \lambda_5 = 0,\ \lambda_6 = -1,$$
$$v_{1,2} = e_1 + (-1 \pm \sqrt{3}i)e_4/2,\ v_{3,4} = e_2 + (-1 \pm \sqrt{3}i)e_5/2,$$
$$v_5 = e_3, \quad v_6 = e_6,$$

where $e_i \in \mathbb{R}^6$ denotes the unit-vector whose i-th element is one, and other elements are zeros. Note that there are repeated eigenvalues, but we obtain six linearly independent eigenvectors, i.e., the geometric multiplicities are equal to the algebraic multiplicities.

The basis of the null space of the matrix C, namely $\mathcal{N}(C)$ is $\{e_1, e_2, e_4, e_5\}$. The solution of the linearized equation can be written as $x(t) = \sum_{i=1}^6 c_i \exp(\lambda_i t) v_i$ for constants c_i that are determined by the initial condition: $x(0) = \sum_{i=1}^6 c_i v_i$. But, the eigenvectors v_5, v_6 do not satisfy the constraint given by (7), since they do not lie in $\mathcal{N}(C)$. Therefore, the constants c_5, c_6 are zero for initial conditions that are compatible with (7). We have $\mathrm{Re}[\lambda_i] < 0$ for $1 \leq i \leq 4$. Therefore, the hanging equilibrium is asymptotically stable.

2) Inverted Equilibrium: The eigenvalues λ_i, and the eigenvectors v_i of the matrix A at the inverted equilibrium $(-e_3, 0)$ are given by

$$\lambda_{1,2} = -(\sqrt{5}+1)/2, \lambda_{3,4} = (\sqrt{5}-1)/2, \lambda_5 = 0, \lambda_6 = -1,$$
$$v_1 = e_1 - (\sqrt{5}+1)e_4/2,\ v_2 = e_2 - (\sqrt{5}+1)e_5/2, \tag{8}$$
$$v_3 = (\sqrt{5}+1)e_1/2 + e_4,\ v_4 = (\sqrt{5}+1)e_2/2 + e_5,$$
$$v_5 = e_3,\ v_6 = e_6.$$

The basis of $\mathcal{N}(C)$ is $\{e_1, e_2, e_4, e_5\}$. Hence, the eigenvectors v_5, v_6 do not lie in $\mathcal{N}(C)$. Therefore, the solution can be written as $x(t) = \sum_{i=1}^4 c_i \exp(\lambda_i t) v_i$ for constants c_i that are determined by the initial condition.

We have $\mathrm{Re}[\lambda_{1,2}] < 0$, and $\mathrm{Re}[\lambda_{3,4}] > 0$. Therefore, the inverted equilibrium $(q, \omega) = (-e_3, 0)$ is a hyperbolic equilibrium, and in particular, a saddle equilibrium.

D. Stable Manifold for the Inverted Equilibrium

1) Stable Manifold: The saddle equilibrium $(-e_3, 0)$ has a stable manifold W^s, which is defined to be

$$W^s(-e_3, 0) = \{(q, \omega) \in \mathsf{TS}^2 \mid \lim_{t\to\infty} \mathcal{F}^t(q, \omega) = (-e_3, 0)\},$$

where $\mathcal{F}^t : (q(0), \omega(0)) \to (q(t), \omega(t))$ denotes the flow map along the solution of (1), (2). The existence of $W^s(-e_3, 0)$ has nontrivial effects on the overall dynamics of the controlled system. Trajectories in $W^s(-e_3, 0)$ converge to the antipodal point of the desired equilibrium $(e_3, 0)$, and it takes a long time period for any trajectory near $W^s(-e_3, 0)$ to asymptotically converge to the desired equilibrium $(e_3, 0)$.

According to the stable and unstable manifold theorem [9], a local stable manifold $W^s_{loc}(-e_3, 0)$ exists in the neighborhood of $(-e_3, 0)$, and it is tangent to the stable eigenspace $E^s(-e_3, 0)$ spanned by the eigenvectors v_1 and v_2 of the stable eigenvalues $\lambda_{1,2}$. Then, the (global) stable manifold can be written as

$$W^s(-e_3, 0) = \bigcup_{t>0} \mathcal{F}^{-t}(W^s_{loc}(-e_3, 0)), \tag{9}$$

which states that the stable manifold W^s can be obtained by globalizing the local stable manifold W^s_{loc} by the backward flow map.

This yields a method to compute $W^s(-e_3, 0)$ [10]. We choose a small ball $B_\delta \subset W^s_{loc}(-e_3, 0)$ with a radius δ around $(-e_3, 0)$, and we grow the manifold $W^s(-e_3, 0)$ by evolving B_δ under the flow $\mathcal{F}^{-t}$. More explicitly, the stable manifold can be parameterized by t as follows:

$$W^s(-e_3, 0) = \{\mathcal{F}^{-t}(B_\delta)\}_{t>0}. \tag{10}$$

A ball B_δ in the local stable manifold can be easily chosen from the stable eigenspace of $(-e_3, 0)$ with a sufficiently small radius δ. Using the stable eigenvectors v_1, v_2 at (8), $E^s_{loc}(-e_3, 0)$ can be written as

$$\begin{aligned} E^s_{loc}(-e_3, 0) = \{(q, \omega) \in \mathsf{TS}^2 \,|\, q = \exp(\alpha_1 \hat{e}_1 + \alpha_2 \hat{e}_2)(-e_3), \\ \omega = -\hat{q}^2(-(\sqrt{5}+1)/2)(\alpha_1 e_1 + \alpha_2 e_2) \text{ for } \alpha_1, \alpha_2 \in \mathbb{R}\}, \end{aligned} \tag{11}$$

where $-\hat{q}^2$ in the expression for ω corresponds to the orthogonal projection onto the plane normal to q, as required due to the constraint $q \cdot \omega = 0$. We define a distance on TS^2 as follows:

$$d_{\mathsf{TS}^2}((q_1, \omega_1), (q_2, \omega_2)) = \sqrt{\Psi(q_1, q_2)} + \|\omega_1 - \omega_2\|. \tag{12}$$

Then, for a sufficiently small $\delta > 0$, B_δ is expressed as (11), where the parameters α_1, α_2 are chosen such that the distance from the elements on B_δ to $(-e_3, 0)$ becomes δ.

2) Variational Integrators: The parameterization of the stable manifold W_s at (10) also requires the computation of the backward flow map $\mathcal{F}^{-t}$. General purpose numerical integrators may not preserve the structure of the two-sphere or the underlying dynamic characteristics, such as energy dissipation rate, accurately, and they may yield qualitatively incorrect numerical results in simulating a complex trajectory over a long-time period [11].

Geometric numerical integration is concerned with developing numerical integrators that preserve geometric features of a system, such as invariants, symmetry, and reversibility. In particular, variational integrators are geometric numerical integrators for Lagrangian or Hamiltonian systems, constructed according to Hamilton's principle. They have the desirable computational properties of preserving symplecticity and momentum maps, and they exhibit good energy behavior [12]. A variational integrator has been developed for Lagrangian or Hamiltonian systems evolving on the two-sphere in [7]. It preserves both the underlying symplectic properties and the structure of the two-sphere concurrently. Here we rewrite the integrator equations in a backward form, and we use it to compute the backward flow map (see [8] for details).

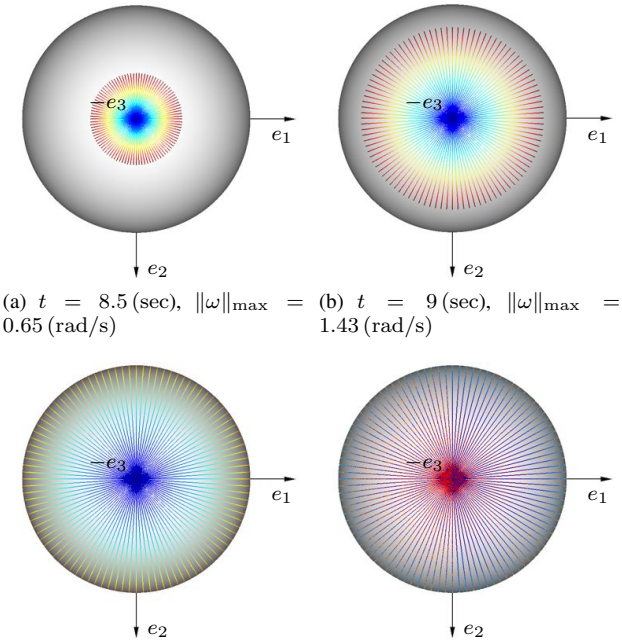

(a) $t = 8.5$ (sec), $\|\omega\|_{\max} = 0.65$ (rad/s) (b) $t = 9$ (sec), $\|\omega\|_{\max} = 1.43$ (rad/s)

(c) $t = 8.5$ (sec), $\|\omega\|_{\max} = 2.96$ (rad/s) (d) $t = 9$ (sec), $\|\omega\|_{\max} = 8.02$ (rad/s)

Fig. 1. Stable manifold to $(q, \omega) = (-e_3, 0)$ represented by $\{\mathcal{F}^{-t}(B_\delta)\}_{t>0}$ for several values of t. One hundred points of B_δ in the stable eigenspace to $(-e_3, 0)$ are chosen with $\delta = 10^{-6}$, and they are integrated backward in time. Each trajectory is illustrated on a sphere, where the magnitude of angular velocity at each point is denoted by color shading (red: $\|\omega\|_{\max}$, blue: $\|\omega\|_{\min} \simeq 0$).

3) Visualization: We choose 100 points on the surface of B_δ with $\delta = 10^{-6}$, and each point is integrated backward using a variational integrator with a timestep of 0.002 seconds. The resulting trajectories are illustrated in Fig. 1 for several values of t. Each colored curve on the sphere represents a trajectory on TS^2, since at any point q on the curve, the direction of $\dot{q}$ is tangent to the curve at q, and the magnitude of $\dot{q}$ is indirectly represented by color shading.

We observe the following characteristics of the stable manifold $W_s(-e_3, 0)$ of the inverted equilibrium:

- The boundary of the stable manifold $W_s(-e_3, 0) \subset \mathsf{TS}^2$ parameterized by t is circular when projected onto S^2.
- Each trajectory in $W_s(-e_3, 0)$ lies on a great circle, when projected onto S^2. According to the closed loop dynamics (1), and the given initial condition at the surface of B_δ, the direction of $\dot{\omega}$ is always parallel to ω. Therefore, the direction of ω is fixed, and the resulting trajectory of q is on a great circle. This also corresponds to the fact that the

eigenvalue λ_1 for the first mode representing the rotations about the first axis is equal to the eigenvalue λ_2 for the second mode representing the rotations about the second axis at (8), i.e. the convergence rates of these two rotations are identical.
- The angular velocity decreases to zero as the direction of the pendulum q converges to $-e_3$.
- The stable manifold $W_s(-e_3, 0)$ may cover S^2 multiple times if t is sufficiently large, as illustrated at Fig. 1(d). Therefore, at any point $q \in \mathsf{S}^2$, we can choose ω such that (q, ω) lies in the stable manifold $W^s(-e_3, 0)$ (the corresponding value of ω is not unique, since if it is sufficiently large, q can traverse the sphere several times before converging to $-e_3$).

The stable manifold $W_s(-e_3, 0)$ to the inverted equilibrium has zero measure in TS^2, but as we illustrate by this example, it may cover S^2 multiple times. This has strong effects on the overall flow of the controlled system, as a trajectory has a slower convergence rate the closer it is to $W_s(-e_3, 0)$.

III. 3D Pendulum

A 3D pendulum is a rigid body supported by a frictionless pivot acting under a gravitational potential. This is a generalization of a planar pendulum or a spherical pendulum, as it has three rotational degrees of freedom. It has been shown that a 3D pendulum may exhibit irregular trajectories [13].

We choose a reference frame, and a body-fixed frame. The origin of the body-fixed frame is located at the pivot point. The attitude of a 3D pendulum is the orientation of the body-fixed frame with respect to the reference frame, and it is described by a rotation matrix representing the linear transformation from the body-fixed frame to the reference frame. The configuration manifold is the special orthogonal group, $\mathsf{SO(3)} = \{R \in \mathbb{R}^{3\times 3} \,|\, R^T R = I, \det[R] = 1\}$.

The equations of motion for a 3D pendulum are given by

$$J\dot{\Omega} + \Omega \times J\Omega = mg\rho \times R^T e_3 + u,$$
$$\dot{R} = R\hat{\Omega},$$

where the matrix $J \in \mathbb{R}^{3\times 3}$ is the inertia matrix of the pendulum about the pivot, and $\rho \in \mathbb{R}^3$ is the vector from the pivot to the center of mass of the pendulum. The angular velocity and the control moment at the pivot are denoted by $\Omega, u \in \mathbb{R}^3$, respectively. They are represented in the body fixed frame.

A. Control System

Several control systems have been developed on $\mathsf{SO(3)}$ [3], [6], [14]. Here, we summarize a control system to stabilize a 3D pendulum to a fixed desired attitude $R_d \in \mathsf{SO(3)}$. Consider an attitude error function given by

$$\Psi(R, R_d) = \frac{1}{2}\mathrm{tr}\big[(I - R_d^T R)G\big],$$

for a diagonal matrix $G = \mathrm{diag}[g_1, g_2, g_3] \in \mathbb{R}^{3\times 3}$ with $g_1, g_2, g_3 > 0$. The derivative of this attitude error function with respect to R along the direction of $\delta R = R\hat{\eta}$ for $\eta \in \mathbb{R}^3$ is given by

$$\mathbf{D}_R\Psi(R, R_d) \cdot \delta R = e_R \cdot \eta,$$

where the *vee map*, $\vee : \mathfrak{so}(3) \to \mathbb{R}^3$, denotes the inverse of the hat map. An attitude error vector is defined as $e_R = \frac{1}{2}(GR_d^T R - R^T R_d G) \in \mathbb{R}^3$. For positive constants k_Ω, k_R, we choose the following control input consisting of terms proportional to the attitude error vector and the angular velocity vector and a cancellation term:

$$u = -k_R e_R - k_\Omega \Omega - mg\rho \times R^T e_3.$$

The corresponding closed loop dynamics are given by

$$J\dot{\Omega} = -\Omega \times J\Omega - k_R e_R - k_\Omega \Omega, \tag{13}$$
$$\dot{R} = R\hat{\Omega}. \tag{14}$$

This system has four equilibria: in addition to the desired equilibrium $(R_d, 0)$, there exist three other equilibria at $(R_d \exp(\pi\hat{e}_i), 0), 0)$ for $i \in \{1, 2, 3\}$, which correspond to the rotation of the desired attitude by 180° about each body-fixed axis. The existence of additional, undesirable equilibria is due to the nontrivial topological structure of $\mathsf{SO(3)}$, and it cannot be avoided by constructing a different control system (as long as it is continuous). It has been shown that it is not possible to design a continuous feedback control stabilizing an attitude globally on $\mathsf{SO(3)}$ [4], [15].

In this paper, we linearize the closed loop dynamics to study the stability of each equilibrium.

B. Linearization

A variation in $\mathsf{SO(3)}$ can be expressed as:

$$R^\epsilon = R\exp(\epsilon\hat{\eta}), \quad \Omega^\epsilon = \Omega + \epsilon\delta\Omega, \tag{15}$$

for $\eta, \delta\Omega \in \mathbb{R}^3$. The corresponding infinitesimal variation of R is given by $\delta R = R\hat{\eta}$. Substituting these into (13), (14), we obtain the linearized equation as follows:

$$\dot{x} = \begin{bmatrix} \dot{\eta} \\ \delta\dot{\Omega} \end{bmatrix} = \begin{bmatrix} -\hat{\Omega} & I \\ -\frac{1}{2}k_R J^{-1} H & J^{-1}(\widehat{J\Omega} - \hat{\Omega}J - k_\Omega I) \end{bmatrix} \begin{bmatrix} \eta \\ \delta\Omega \end{bmatrix}$$
$$= Ax, \tag{16}$$

where $H = \mathrm{tr}[R^T R_d G]I - R^T R_d G \in \mathbb{R}^{3\times 3}$ (see [8] for details).

C. Equilibrium Solutions

We choose the desired attitude as $R_d = I$. In addition to the desired equilibrium $(I, 0)$, there are three additional equilibria, namely $(\exp(\pi\hat{e}_1), 0)$, $(\exp(\pi\hat{e}_2), 0)$, $(\exp(\pi\hat{e}_3), 0)$. We assume that

$$J = \mathrm{diag}[3, 2, 1]\,\mathrm{kgm}^2,\ G = \mathrm{diag}[0.9, 1, 1.1],\ k_R = k_\Omega = 1.$$

1) Equilibrium $(I, 0)$*:* The eigenvalues of the matrix A at the desired equilibrium $(I, 0)$ are given by

$$\lambda_{1,2} = -0.1667 \pm 0.5676i,$$
$$\lambda_{3,4} = -0.25 \pm 0.6614i,$$
$$\lambda_{5,6} = -0.5 \pm 0.8367i.$$

This equilibrium is an asymptotically stable focus.

2) Equilibrium $(\exp(\pi\hat{e}_1), 0)$*:* At this equilibrium, the eigenvalues and the eigenvectors of A are given by

$$\begin{aligned} \lambda_1 &= -0.7813, \quad v_1 = e_1 + \lambda_1 e_4, \\ \lambda_2 &= -0.5854, \quad v_2 = e_2 + \lambda_2 e_5, \\ \lambda_3 &= -1.0477, \quad v_3 = e_3 + \lambda_3 e_6, \\ \lambda_4 &= 0.4480, \quad v_4 = e_1 + \lambda_4 e_4, \\ \lambda_5 &= 0.0854, \quad v_5 = e_2 + \lambda_5 e_5, \\ \lambda_6 &= 0.0477, \quad v_6 = e_3 + \lambda_6 e_6. \end{aligned} \tag{17}$$

Therefore, this equilibrium is a saddle equilibrium, where three modes are stable, and three modes are unstable.

3) Equilibrium $(\exp(\pi\hat{e}_2), 0)$*:* At this equilibrium, the eigenvalues and the eigenvectors of A are given by

$$\begin{aligned} \lambda_1 &= -0.3775, \quad v_1 = e_1 + \lambda_1 e_4, \\ \lambda_2 &= -1, \quad v_2 = e_2 + \lambda_2 e_5, \\ \lambda_3 &= -0.9472, \quad v_3 = e_3 + \lambda_3 e_6, \\ \lambda_4 &= -0.0528, \quad v_4 = e_3 + \lambda_4 e_6, \\ \lambda_5 &= 0.0442, \quad v_5 = e_1 + \lambda_5 e_4, \\ \lambda_6 &= 0.5, \quad v_6 = e_2 + \lambda_6 e_5. \end{aligned} \tag{18}$$

Therefore, this equilibrium is a saddle equilibrium, where four modes are stable, and two modes are unstable.

4) Equilibrium $(\exp(\pi\hat{e}_3), 0)$*:* At this equilibrium, the eigenvalues and the eigenvectors of A are given by

$$\begin{aligned} \lambda_1 &= -0.0613, \quad v_1 = e_1 + \lambda_1 e_4, \\ \lambda_2 &= -0.2721, \quad v_2 = e_1 + \lambda_2 e_4, \\ \lambda_3 &= -0.1382, \quad v_3 = e_2 + \lambda_3 e_5, \\ \lambda_4 &= -0.3618, \quad v_4 = e_2 + \lambda_4 e_5, \\ \lambda_5 &= -1.5954, \quad v_5 = e_3 + \lambda_5 e_6, \\ \lambda_6 &= 0.5954, \quad v_6 = e_2 + \lambda_6 e_6. \end{aligned} \tag{19}$$

Therefore, this equilibrium is a saddle equilibrium, where five modes are stable, and one mode is unstable.

D. Stable Manifolds for the Saddle Equilibria

Eigen-structure analysis shows that there exist multi-dimensional stable manifolds for each saddle equilibrium. They have zero measure as the dimension of the stable manifold is less than the dimension of $\mathsf{TSO(3)}$. But, the existence of these stable manifolds may have nontrivial effects on the attitude dynamics. We numerically characterize these stable manifolds using backward time integration, as discussed in Section II-D.

The stable eigenspace for each saddle equilibrium can be written in terms of eigenvectors similar to (11). For example, the stable eigenspace for $(\exp(\pi\hat{e}_3), 0)$ is given by

$$\begin{aligned} &E^s_{loc}(\exp(\pi\hat{e}_3), 0) = \{(R, \Omega) \in \mathsf{TSO(3)} \,|\, \\ &R = \exp(\pi\hat{e}_3)\exp((\alpha_1+\alpha_2)\hat{e}_1 + (\alpha_3+\alpha_4)\hat{e}_2 + \alpha_5\hat{e}_3), \\ &\Omega = (\lambda_1\alpha_1 + \lambda_2\alpha_2)e_1 + (\lambda_3\alpha_3 + \lambda_4\alpha_4)e_2 \\ &\quad - \lambda_5\alpha_5 e_3 \text{ for } \alpha_i \in \mathbb{R}\}, \end{aligned}$$

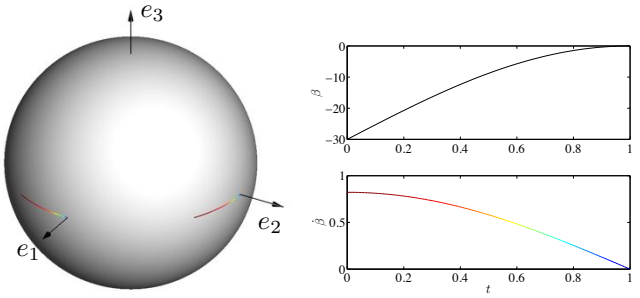

(a) Visualization on sphere (b) Rotation angle β (deg), and rotation rate $\dot{\beta}$ (rad/sec)

Fig. 3. Visualization of an attitude maneuver: $R(t) = \exp(\beta(t)\hat{e}_3)$ for $0 \le t \le 1$, where $\beta(t) = \frac{\pi}{6}(\sin\frac{\pi}{2}t - 1)$. This maneuver corresponds to a rotation about the e_3 axis by 30° to $R(1) = I$. The trajectory of the i-th column of $R(t)$ representing the direction of the i-th body-fixed axis is illustrated on a sphere for $i \in \{1, 2, 3\}$ (left). As the third body-fixed axis does not move during this maneuver, it is represented by a single point along the e_3 axis on the sphere. The direction of $\dot{R}(t)$ is tangent to these curves, and the magnitude of $\dot{R}(t)$ is denoted by color shading, according to the magnitude of the rotation rate (right).

We define a distance on $\mathsf{TSO(3)}$ as follows:

$$d_{\mathsf{TSO(3)}}((R_1, \Omega_1), (R_2, \Omega_2)) = \sqrt{\Psi(R_1, R_2)} + \|\Omega_1 - \Omega_2\|.$$

A variational integrator for the attitude dynamics of a rigid body on $\mathsf{SO(3)}$ has been developed in [16]. In this paper, we rewrite is as a backward integration form, and we use it to compute the backward flow map (see [8] for details).

1) Visualization of $W_s(\exp(\pi\hat{e}_1), 0)$*:* In [17], a method to visualize a function or a trajectory on $\mathsf{SO(3)}$ is proposed. Each column of a rotation matrix represents the direction of a body-fixed axis, and it evolves on S^2. Therefore, a trajectory on $\mathsf{SO(3)}$ can be visualized by three curves on a sphere, representing the trajectory of three columns of a rotation matrix. The direction of the angular velocity should be chosen such that the corresponding time-derivative of the rotation matrix is tangent to the curve, and the magnitude of angular velocity can be illustrated by color shading. An example of visualizing a rotation about a single axis is illustrated in Fig. 3.

We choose 112 points on the surface of $B_\delta \subset E^s_{loc}(\exp(\pi\hat{e}_1), 0)$ with $\delta = 10^{-6}$, and each point is integrated backward. The resulting trajectories are illustrated in Fig. 2 for several values of t.

In each figure, three body-fixed axes of the desired attitude $R_d = [e_1, e_2, e_3]$, and three body-fixed axes of the additional equilibrium attitude $\exp(\pi\hat{e}_1) = [e_1, -e_2, -e_3]$ are shown. From these computational results, we observe the following characteristics on the stable manifold $W_s(\exp(\pi\hat{e}_1), 0)$:

- When $t \le 15$, the trajectories in $W_s(\exp(\pi\hat{e}_1), 0)$ are close to rotations about the third body-fixed axis e_3 to $\exp(\pi\hat{e}_1)$. This is consistent with the linearized dynamics, where the eigenvalue of the third mode, corresponding to the rotations about e_3, has the fastest convergence rate, as seen in (17).
- When $t \ge 15$, the first mode representing the rotations about e_1 starts to appear, followed by the second mode

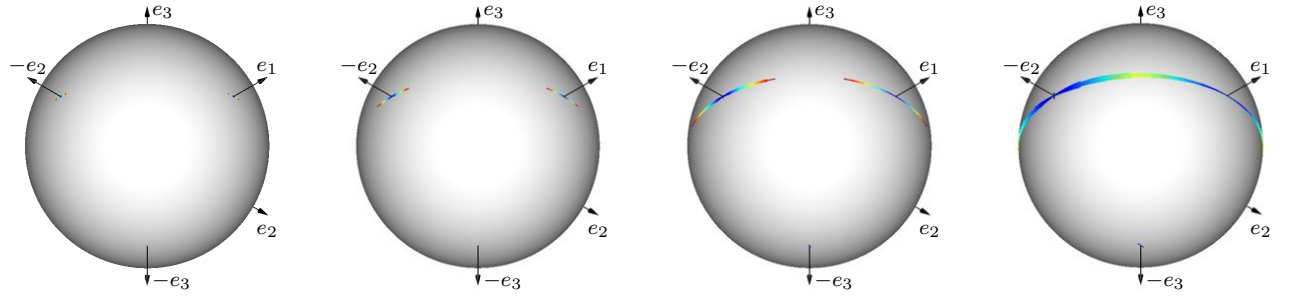

(a) $t = 11$ (sec), $\|\Omega\|_{\max} = 0.06$ (rad/s) (b) $t = 12$ (sec), $\|\Omega\|_{\max} = 0.17$ (rad/s) (c) $t = 13$ (sec), $\|\Omega\|_{\max} = 0.50$ (rad/s) (d) $t = 14$ (sec), $\|\Omega\|_{\max} = 1.42$ (rad/s)

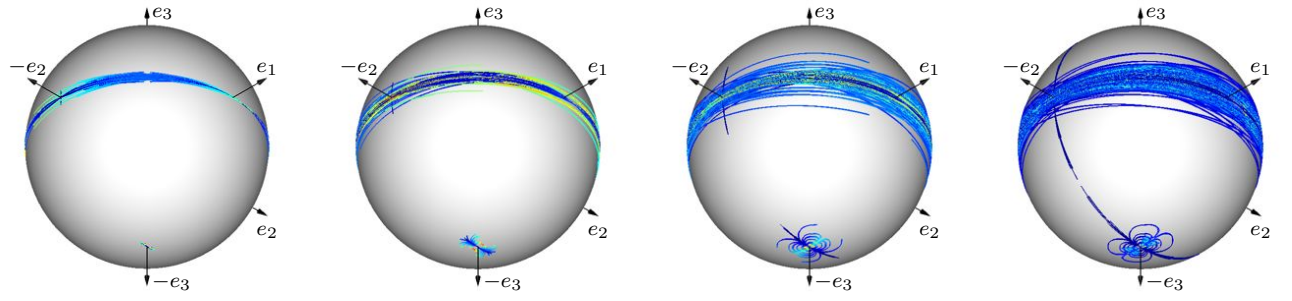

(e) $t = 15$ (sec), $\|\Omega\|_{\max} = 3.93$ (rad/s) (f) $t = 16$ (sec), $\|\Omega\|_{\max} = 10.67$ (rad/s) (g) $t = 17$ (sec), $\|\Omega\|_{\max} = 29.00$ (rad/s) (h) $t = 18$ (sec), $\|\Omega\|_{\max} = 78.84$ (rad/s)

Fig. 2. Stable manifold to $(\exp(\pi\hat{e}_1), 0) = ([e_1, -e_2, -e_3], 0)$ represented by $\{\mathcal{F}^{-t}(B_\delta)\}_{t>0}$ with $\delta = 10^{-6}$ for several values of t.

representing the rotation about e_2. This corresponds to the fact that the first mode has a faster convergence rate than the second mode, i.e. $|\lambda_1| > |\lambda_2|$.

- As t is increased further, the third body-fixed axis leaves the neighborhood of $-e_3$, and it exhibit the following pattern:

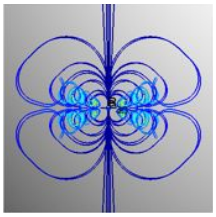

- The stable manifold $W_s(\exp(\pi\hat{e}_1), 0)$ covers a certain part of $\mathsf{SO(3)}$, when projected on to it. So, when an initial attitude is chosen such that its third body-fixed axis is sufficiently close to $-e_3$, there possibly exist multiple initial angular velocities such that the corresponding solution converges to $\exp(\pi\hat{e}_1)$ instead of the desired attitude, I.

2) Visualization of $W_s(\exp(\pi\hat{e}_2), 0)$: Similarly, we compute $W_s(\exp(\pi\hat{e}_2), 0)$ from 544 points. The resulting trajectories are illustrated in Fig. 4 for several values of t. From these computational results, we observe the following characteristics on the stable manifold $W_s(\exp(\pi\hat{e}_2), 0)$:

- When $t \leq 12$, the trajectories in $W_s(\exp(\pi\hat{e}_2), 0)$ is close to the rotations about the second body-fixed axis e_2. As t increases, rotations about e_3 starts to appear. This corresponds to the linearized dynamics where the second mode representing rotations about e_2 has the fastest convergence rate, followed by the third mode at (18).
- As t is increased further, nonlinear modes become dominant. The trajectories in $W_s(\exp(\pi\hat{e}_2), 0)$ almost cover $\mathsf{SO(3)}$. This suggests that for any initial attitude, we can choose several initial angular velocities such that the corresponding solutions converges to $\exp(\pi\hat{e}_2)$.

3) Visualization of $W_s(\exp(\pi\hat{e}_3), 0)$: We also compute $W_s(\exp(\pi\hat{e}_3), 0)$ from 976 points. The resulting trajectories are illustrated in Fig. 5 for several values of t. From these computational results, we observe the following characteristics on the stable manifold $W_s(\exp(\pi\hat{e}_3), 0)$:

- When $t \leq 8$, the trajectories in $W_s(\exp(\pi\hat{e}_3), 0)$ are close to the rotations about the third body-fixed axis e_3. This corresponds to the linearized dynamics where the fifth mode representing rotations about e_3 has the fastest convergence rate given in (19).
- The rotations about e_3 are still dominant, even as t is increased further. For the given simulation times, all trajectories are close to rotations about e_3.

In a 3D Pendulum, the characteristics of stable manifolds can vary widely depending on the equilibria. We observe that $W_s(\exp(\pi\hat{e}_3), 0)$ has a higher dimension, but it has simpler trajectories over the time period considered in this paper. The trajectories in $W_s(\exp(\pi\hat{e}_2), 0)$ are most complicated, and they cover a large part of $\mathsf{SO(3)}$. This illustrates that the existence of stable manifolds of the saddle equilibria has important effects to the global dynamics of the controlled system.

REFERENCES

[1] N. A. Chaturvedi, A. K. Sanyal, and N. H. McClamroch, "Rigid body attitude control: Using rotation matrices for continuous, singularity-free control laws," *IEEE Control Systems Magazine*, pp. 30–51, 2011.

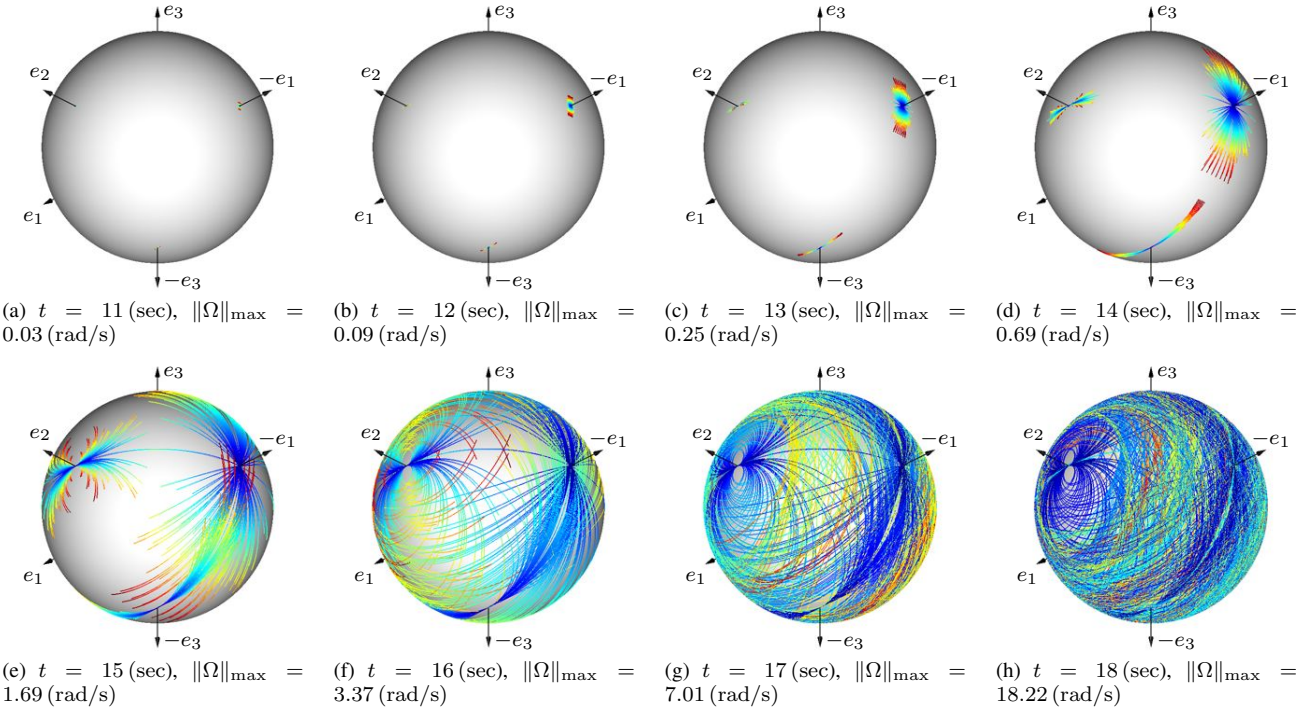

(a) $t = 11\,(\text{sec})$, $\|\Omega\|_{\max} = 0.03\,(\text{rad/s})$ (b) $t = 12\,(\text{sec})$, $\|\Omega\|_{\max} = 0.09\,(\text{rad/s})$ (c) $t = 13\,(\text{sec})$, $\|\Omega\|_{\max} = 0.25\,(\text{rad/s})$ (d) $t = 14\,(\text{sec})$, $\|\Omega\|_{\max} = 0.69\,(\text{rad/s})$

(e) $t = 15\,(\text{sec})$, $\|\Omega\|_{\max} = 1.69\,(\text{rad/s})$ (f) $t = 16\,(\text{sec})$, $\|\Omega\|_{\max} = 3.37\,(\text{rad/s})$ (g) $t = 17\,(\text{sec})$, $\|\Omega\|_{\max} = 7.01\,(\text{rad/s})$ (h) $t = 18\,(\text{sec})$, $\|\Omega\|_{\max} = 18.22\,(\text{rad/s})$

Fig. 4. Stable manifold to $(\exp(\pi\hat{e}_2), 0) = ([-e_1, e_2, -e_3], 0)$ represented by $\{\mathcal{F}^{-t}(B_\delta)\}_{t>0}$ with $\delta = 10^{-6}$ for several values of t.

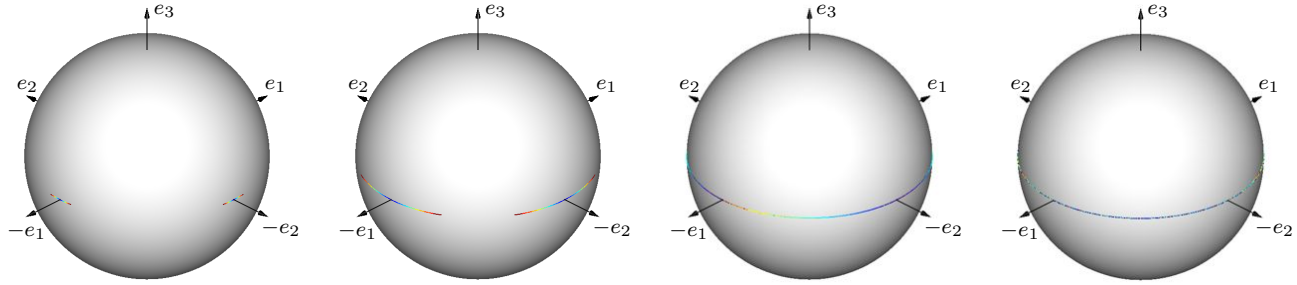

(a) $t = 8\,(\text{sec})$, $\|\Omega\|_{\max} = 0.224\,(\text{rad/s})$ (b) $t = 9\,(\text{sec})$, $\|\Omega\|_{\max} = 1.09\,(\text{rad/s})$ (c) $t = 10\,(\text{sec})$, $\|\Omega\|_{\max} = 4.26\,(\text{rad/s})$ (d) $t = 14\,(\text{sec})$, $\|\Omega\|_{\max} = 222.99\,(\text{rad/s})$

Fig. 5. Stable manifold to $(\exp(\pi\hat{e}_3), 0) = ([-e_1, -e_2, e_3], 0)$ represented by $\{\mathcal{F}^{-t}(B_\delta)\}_{t>0}$ with $\delta = 10^{-6}$ for several values of t.

[2] N. A. Chaturvedi, N. H. McClamroch, and D. S. Bernstein, "Stabilization of a 3D axially symmetric pendulum," *Automatica*, pp. 2258–2265, 2008.

[3] N. Chaturvedi, N. H. McClamroch, and D. Bernstein, "Asymptotic smooth stabilization of the inverted 3-D pendulum," *IEEE Transactions on Automatic Control*, vol. 54, no. 6, pp. 1204–1215, 2009.

[4] D. Koditschek, "Application of a new lyapunov function to global adaptive tracking," in *Proceedings of the IEEE Conference on Decision and Control*, 1998, pp. 63–68.

[5] F. Bullo, R. M. Murray, and A. Sarti, "Control on the sphere and reduced attitude stabilization," in *IFAC Symposium on Nonlinear Control Systems*, vol. 2, 1995, pp. 495–501.

[6] F. Bullo and A. Lewis, *Geometric control of mechanical systems*. Springer, 2005.

[7] T. Lee, M. Leok, and N. H. McClamroch, "Lagrangian mechanics and variational integrators on two-spheres," *International Journal for Numerical Methods in Engineering*, vol. 79, pp. 1147–1174, 2009.

[8] T. Lee, M. Leok, and N. McClamroch, "Stable manifolds of saddle points for pendulum dynamics on S^2 and $\mathsf{SO(3)}$," arXiv:1103.2822v1. [Online]. Available: http://arxiv.org/abs/1103.2822v1

[9] Y. Kuznetsov, *Elements of Applied Bifurcation Theory*. Springer, 1998.

[10] B. Krauskopf, H. Osinga, E. Doedel, M. Henderson, J. Guckenheimer, A. Vladimirsky, M. Dellnitz, and O. Junge, "A survey of methods for computing (un)stable manifolds of vector fields a survey of methods for computing (un)stable manifolds of vector fields," *International Journal of Bifurcation and Chaos*, vol. 15, no. 3, pp. 763–791, 2005.

[11] E. Hairer, C. Lubich, and G. Wanner, *Geometric numerical integration*, ser. Springer Series in Computational Mechanics 31. Springer, 2000.

[12] J. Marsden and M. West, "Discrete mechanics and variational integrators," in *Acta Numerica*. Cambridge, 2001, vol. 10, pp. 317–514.

[13] N. Chaturvedi, T. Lee, M. Leok, and N. H. McClamroch, "Nonlinear dynamics of the 3D pendulum," *Journal of Nonlinear Science*, vol. 21, no. 1, pp. 3–21, 2011.

[14] T. Lee, "Geometric tracking control of the attitude dynamics of a rigid body on SO(3)," in *Proceeding of the American Control Conference*, 2011, pp. 1885–1891.

[15] S. Bhat and D. Bernstein, "A topological obstruction to continuous global stabilization of rotational motion and the unwinding phenomenon," *Systems and Control Letters*, vol. 39, pp. 66–73, 2000.

[16] T. Lee, M. Leok, and N. H. McClamroch, "Lie group variational integrators for the full body problem in orbital mechanics," *Celestial Mechanics and Dynamical Astronomy*, vol. 98, pp. 121–144, 2007.

[17] ——, "Global symplectic uncertainty propagation on SO(3)," in *Proceedings of the IEEE Conference on Decision and Control*, 2008, pp. 61–66.